Large Eddy Simulations of Reacting Flows in a Dump Combustor[†]

Won-Wook Kim[‡], Suresh Menon[††]
Georgia Institute of Technology
Atlanta, GA, 30332-0150, USA
and
Hukam C. Mongia[‡‡]
General Electric Aircraft Engines
Cincinnati, OH 45215, USA

Abstract

Large-eddy simulations (LES) of turbulent premixed combustion in a dump combustor that is an accurate model for an actual gas turbine combustor (General Electric's lean premixed dry low NOx LM-6000) has been carried out to evaluate the potential of LES for design studies of realistic hardware. A thin flame model for the premixed flame is combined with a dynamic model for the subgrid kinetics energy to simulate the propagation of the turbulent flame in this highly swirling and high Reynolds number flow field. Comparison of the computed results with experimental data indicate very good agreement in spite of relatively coarse grid resolution employed in the LES. These results provide significant confidence that advanced parallel LES capability for design studies of practical interest is feasible in the near future.

Introduction

Time-accurate simulation of turbulent flames in high Reynolds number flows is a challenging task since both fluid dynamics and combustion must be modeled and/or resolved accurately. Direct simulations (in which all scales are resolved and no models are used) are not practical since the resolution and computational resource requirements far exceed the computational capability available at present and possibly in the near future. On the other hand, Reynolds-Averaged methods are not acceptable since they predict the mean motion using a global model for all turbulent scales and ignore the unsteady dynamics which is critical for accurate predictions. In the present study, we explore the ability of large-eddy simulations (LES) for simulating high Reynolds number reacting flows in realistic configurations.

In LES, the scales larger than the grid are computed using a time- and space-accurate scheme, while the unresolved smaller scales are modeled. Since only the small scales are modeled it has been suggested that this approach has the potential for studying relatively high Reynolds number flows. However, most LES applications reported in the past have been limited to simple and/or relatively low Reynolds number flows. The present study employs LES to study turbulent premixed combustion in a combustor which is a part of an operational hardware. In particular, the device that is investigated here is the LM-6000 lean premixed dry low-NOx combustor being developed by General Electric Aircraft Engine Company for gas turbine applications (Hura et al., 1998; Held et al., 1998a,b). Thus, the present demonstration is a focussed "engineering" evaluation of the capability of LES to simulate combustion in realistic hardware. A key requirement for "engineering" LES is that such simulations have to be completed in a reasonable time-frame. This implies that both the accuracy of the methodology and the computational effort involved has to be evaluated.

The primary focus of this study is on the development of a new Computational Combustion Dynamics (CCD) tool based on LES for realistic combustor design. To date, this type of design tool has been considered impractical primarily due to the immaturity of LES methodology for practical engineering problems and the lack of adequate computing resources. With the recent progress in subgrid-scale (SGS) modeling techniques and the availability of massively parallel systems with terraflop capability, these limitations can be tackled using optimized parallel LES codes. This paper explores this capa-

---

‡. Post Doctoral Fellow, Member AIAA
††. Professor, Senior Member AIAA
‡‡. Manager, Combustion Technology, Fellow AIAA

bility and reports on some progress on the development of such a simulation tool. The eventual goal is to develop a design CCD code that can take advantage of the developments in parallel computing architecture so that it can be utilized by industry in the near future.

Simulation Methodology

In the LES approach, the scales larger than the grid are computed using a time- and space-accurate scheme, while the unresolved smaller scales are modeled. The Navier-Stokes equations that govern the conservation of mass, momentum and energy in a fluid are filtered to obtain the LES equations. The filtering operation results in terms in these equations that must be modeled. Closure of momentum and energy transport equations can be achieved using subgrid-scale turbulence models. A localized dynamic model based on the subgrid-scale turbulent kinetic energy has been developed for the closure of the subgrid-scale terms in the momentum and energy equations (Kim and Menon, 1995; Menon and Kim, 1996; Kim and Menon, 1997; Nelson and Menon, 1998). Application of this subgrid model in both incompressible and compressible turbulent flows shows that this model is capable of accurately representing the effect of unresolved terms even when relatively coarse grids are employed. Recently, this model has been compared and evaluated against other contemporary state-of-the-art dynamic models by Fureby *et al.* (1997). The details of the LES equations and the subgrid closure employed are given elsewhere and therefore, only briefly summarized here.

In a multi-component flow field, the key terms that require closure are the stresses in the momentum equations: $\tau_{ij}^{sgs} = \bar{\rho}[\widehat{u_i u_j} - \hat{u}_i \hat{u}_j]$, the energy flux and the viscous terms in the energy equation: $H_i^{sgs} = \bar{\rho}[\widehat{E u_i} - \hat{E}\hat{u}_i] - [\overline{p u_i} - \bar{p}\hat{u}_i]$, $\sigma_{ij}^{sgs} = [\overline{u_i \tau_{ij}} - \hat{u}_i \overline{\tau_{ij}}]$ and the scalar correlations: $\psi_k^{sgs} = \overline{T Y_k} - \bar{T}\hat{Y}_k$ in the equation of state. Here, hat and bar indicate filtered variables, u_i, $\bar{\rho}$, τ_{ij} and E are, respectively, the resolved velocity components, the density, the viscous stresses and the total energy per unit volume. To close these subgrid terms, a model equation for the subgrid kinetic energy $k = \widehat{u_i u_i} - \hat{u}_i \hat{u}_i$ is also solved along with the LES equations (Kim and Menon, 1995; Menon and Kim, 1996). The subgrid terms are then obtained using the subgrid kinetic energy as the characteristic velocity scale and the grid scale as the characteristic length scale. Thus, the eddy viscosity is determined as: $\nu_t = C_\nu k^{1/2} \Delta_g$ where, Δ_g is the grid size. The coefficients in the subgrid kinetic energy equation and in the eddy viscosity form (e.g., C_ν) are computed locally (in space and time) during the simulation using a dynamic procedure that has been discussed elsewhere (e.g., Kim and Menon, 1995, Menon and Kim, 1996; Fureby et al., 1997). With k known, the subgrid terms can be closed. Thus, the subgrid turbulent stresses are modeled as: $\tau_{ij}^{sgs} = -2\bar{\rho}\nu_t(S_{ij} - S_{kk}\delta_{ij}/3)$, the subgrid enthalpy flux is approximated as, $H_i^{sgs} = -\bar{\rho}\nu_t(H)_i / Pt_t$ and $\sigma_{ij}^{sgs} = \hat{u}_j \tau_{ij}^{sgs}$. Here, $Pr \approx 1$ is the turbulent Prandtl number, S_{ij} is the resolved rate-of-strain tensor, $S_{ij} = [(\hat{u}_i)_j + (\hat{u}_j)_i]/2$, and H is the resolved total enthalpy. Also, all third-order subgrid correlations are neglected in this closure for simplicity.

In general, simulation of reacting flows (both premixed and non-premixed) requires the solution of the species conservation equations. The LES species equations can be written as:

$$(\bar{\rho}\hat{Y}_k)_t + (\bar{\rho}\hat{u}_i\hat{Y}_k)_i + \left(\bar{\rho}S_{ik}^{sgs}\right)_i = (\bar{\rho}D_k(\hat{Y}_k)_i)_i + \overline{\omega_k} \quad (1)$$

where, Y_k and D_k are, respectively, the kth species mass fraction and the diffusion coefficient. Here, $(\phi)_t$ and $(\phi)_i$ indicate differentiation with respect to time and space, respectively. Closure for the species-velocity correlation $S_{ik}^{sgs} = \bar{\rho}(\widehat{u_i Y_k} - \hat{u}_i \hat{Y}_k)$, the production term ω_k and the scalar correlations Ψ_k^{sgs} is more problematic, since, to estimate these terms, small-scale turbulent mixing and species molecular diffusion must be modeled correctly. Conventional subgrid closure cannot handle these features and, therefore, the new subgrid combustion models (Menon and Calhoon, 1996; Smith and Menon, 1998) are being developed to address this limitation.

For conventional LES simulations of turbulent premixed combustion, a model which circumvents the

above noted closure problem can be used for simulations of thin flames (i.e., for flames thinner than the smallest eddy). For these cases, the flame is modeled as a propagating surface and a variable G is defined that is governed by the equation (Kerstein et al., 1998):

$$(G)_t + u \bullet \nabla G = -u_F |\nabla G| \qquad (2)$$

where u_F is the local propagation speed. This equation describes the convection of a level surface, described by G = constant, by the velocity u while undergoing propagation normal to itself at a speed u_F. G=1 denotes the reactant and G=0 the burnt region with the thin flame identified by a level surface in the [0,1] range. The effect of heat release is included in the definition of the specific enthalpy. For turbulent flames, the propagation speed u_F is the turbulent flame speed u_T and has to be specified. Earlier (Menon and Jou, 1991) employed the flame speed model of Yakhot (1988) $u_F/S_L = exp[u'^2/u_F^2]$. Here, S_L is the laminar flame speed and $u' = \sqrt{2k/3}$ is the local turbulence intensity which is known.

In the present study, the G-equation model is again employed for the simulation. Interestingly enough, although this model was originally proposed for the flamelet regime, the domain of its applicability appears to be much larger as demonstrated recently by Peters (1998). In the present LES approach, the G evolution equation is filtered in a similar way as is done for Navier-Stokes equations. Two unresolved terms are obtained as a result of filtering: the transport and the source terms, respectively. The unresolved transport term is modeled using a gradient diffusion assumption (Smith and Menon, 1998). For closure of the source term, various models have been developed and proposed, among them is Yakhot's RNG model (Yakhot, 1988) where the turbulent flame speed is analytically expressed as a function of turbulence intensity. Yakhot's model has been tested in the present study and it was found that the predicted turbulent flame speed is too small when the turbulence intensity of the LM-6000 is considered (see more discussion below). This result may be due to the very high swirl intensity in the present problem and is an issue that warrants further investigation. Therefore, to obtain a reasonable turbulent flame speed for the regime of interest, Pocheau's model (Pocheau, 1994) is employed in the following form:

$$u_T = (1 + \beta u'^2)^{1/2} \qquad (3)$$

where β is an adjustable parameter. In the present study, β is calibrated using existing data of weakly swirling premixed turbulent flames (Cheng, 1995). However, the form of the turbulent flame speed model is an issue for further research and some implications of the choice is also discussed in this paper.

Parallel Implementation

The technique of data concurrency (i.e., the primary data space is partitioned and distributed among the processors) rather than functional concurrency (i.e., the overall application is decomposed into several distinct parallel computational tasks) was chosen after careful review of the type and degree of parallelism inherent in the numerical algorithm. The data space is partitioned and distributed to the processors so that 1) the distribution of cells to the nodes leads to a nearly balanced load of communication and computation among all nodes, and 2) the inherent spatial data locality of the underlying cell structure is maintained so as to minimize interprocessor communication. The cell partitioning scheme decomposes the 3D computational domain into logically congruent, nearly equal-sized cubes. Maximum concurrency is extracted to minimize the execution time on a given number of processors. The overheads associated with parallel implementation, such as, (1) load imbalance, (2) inter-processor communication, (3) data dependency delays, (4) arithmetic, and (5) memory, were analyzed. While the first four types of overheads lead to performance degradation, the memory overhead limits the size of the problem that can be executed on a fixed number of processors. In practice, simultaneously minimizing all these overheads is very difficult.

In the present implementation, the partitioning scheme results in each processor performing computations only on the cells that are held by it. For finite-differences, each domain contains extra layers of ghost cells along the processor partitions to allow the exchange of boundary cell data. This exchange is carried out using a few, relatively long messages. As a result, the high cost of latency associated with message passing is minimized, resulting in a reduced communication overhead even though this data exchange results in an increased memory overhead.

The current implementation on parallel systems

employs double precision (64-bit) arithmetic and is based entirely on Fortran. Performance comparison with and without I/O has been carried out. However, I/O overhead is unavoidable since the data generated on the spatio-temporal evolution of the flow field is needed for analysis. The type, form and frequency of data varies with the problem and, thus, cannot be standardized. In general, the 3D flow field is needed for flow visualization and for restart files. The present approach combines both these requirements by making all processors to write the required data into one file. The location of this file depends on system architecture: for example, the file can reside on the local file system or it has to reside on one processor. In general, if each processor writes its own local data the I/O overhead is the minimum; however, this capability is not available in many modern distributed parallel systems such as the Cray T3E.

To optimize I/O time on *all* systems, the flow variables from all processors are written into a temporary buffer array which always resides on one processor and then this array is written to a file. This approach results in one processor writing a large amount of data instead of all processors writing small amounts of data (which was found to cause I/O bottleneck). Recent studies suggest that if a processor is allocated the task of only I/O then asynchronous I/O can be conducted without adversely affecting the computational effort. This I/O implementation works reasonably well on all systems and is considered an optimal compromise to allow flexibility in porting the code (and data) to different systems. In addition, this approach allows the simulation to be restarted on arbitrary number of processors. This capability is very useful when the system is heavily loaded.

The timing data for the present 3D LES code is summarized in Table 1 for the T3E and the Origin 2000. The 3D code achieves 32.33 Mflops per processor on the Cray T3E (when 90 processors were used - see further discussion in the next section). This compares very well with some parallel benchmarks reported for this machine. The present LES code also achieves very good scale-up efficiency on the T3E. However, as is well known the scaleup depends upon the problem size and therefore, the optimum size for a given system configuration needs to be determined. Table 1 also shows that although the computational speed on the O2000 is better (by almost a factor of 2), the scale-up (for a given problem size) is not as good as on the T3E. This is related to the problem size; however, in general, it appears that the O2000 architecture is computationally faster than the T3E but does not maintain good scaleup when the number of processors are increased.

Numerical Model and Test Problem

General Electric's lean premixed dry low NOx emissions LM6000 gas turbine combustor has been simulated. As shown in Fig. 1, this problem has a complicated geometry that is quite challenging for computation. A highly swirling jet (the maximum value of tangential velocity component is slightly greater than the peak value of axial velocity component) is injected from a circular inlet under high pressure (P=6.18x10^5 N/m2 ~ 6 atmospheres) and temperature (T=644 K) conditions. The combustor comprises of a rectangular box with two blocks located at top and bottom surfaces from which cooling air is blown downstream. The typical maximum inflow axial jet velocity is around 110m/s and the Reynolds number based on the maximum velocity is 350,000. The premixed fuel-air mixture has a pre-specified laminar flame speed of 0.28 m/ (corresponding to a lean methane-air mixture). The estimated flame temperature is around 1811 K (based on gaseous emissions). The Reynolds number is high enough such that the flamelet assumption is reasonable for this test case. Estimates suggest that the ratio u'/S_L can be locally as high as 100 in this combustor.

To carry out a true "blind" comparison (and to demonstrate a honest test of the LES model), the present LES was carried out without any knowledge of the experimental data. The only information provided by GEAE was the configurational details noted in fig. 1, non-dimensional inflow velocity profiles (axial, radial, and azimuthal), maximum axial, radial, and azimuthal velocities, and, the inflow turbulence intensity. LES was carried out using around 300,000 (80x48x80) and 500,000 (96x64x80) grid points. These resolutions are considered very coarse and not representative of typical LES reported in the literature. However, this range of resolution size was chosen to obtain "engineering" results in a reasonable time frame. The accuracy of such a resolution choice obviously requires confirmation using both comparison with data and higher grid resolution LES. In the present paper, we demonstrate the current LES capability by direct comparison with data. Higher resolution LES will be carried out in the near future and will be reported soon (Kim et al., 1999).

The LES model is based on a finite-volume scheme that is fourth-order accurate in space and second-order accurate in time. The full compressible LES equations are solved along with the filtered G-equation and the equation for the subgrid kinetic energy. Both the constant coefficient and the dynamic subgrid kinetic energy models were used and the results are compared. A limi-

tation of employing the G-equation is that it has only two possible states: G=1 denoting premixed cold fuel and G=0 denoting the hot products. In the experiments, cold air is blown through the side blocks (see Fig. 1) primarily for cooling the combustor. However, all the combustion process is completed upstream of the air ports. Therefore, in the present G-equation approach, we inject the hot product through the injection port using the same amount of mass flow rate. The consequence of this injection on the combustion process occurring upstream cannot be addressed using the G-equation and requires LES with multi-species. The current LES code does have this capability and we plan to carry out such simulations in the near future.

The coarseness of the grid employed here implies that acceptable resolution in all regions of interest cannot be achieved. Since we were interested in the flame region, the grid was clustered in the near field of the exit plane at the expense of the resolution near the wall and far downstream. As a result, the dynamic model has numerical problem near the wall. To stabilize the dynamic simulations, the constant coefficient version is employed near the wall region. The consequence of coarse grid near the wall is that some of the derived properties are not likely to be accurate near this region (see the next section). Higher resolution simulations are planned to revisit this issue.

The inflow conditions were specified based on the normalized profiles provided by GEAE. No data on the incoming turbulence was available or provided (other than the incoming intensity of 7%). In the present study, an inflow turbulent field was generated by specifying the turbulence intensity. The outflow was quite problematic initially, since, due to the high swirl in the flowfield, reverse flow can occur near the outflow during the initial start-up transients. To avoid this problem, a buffer region of 7.6 cm was added in the axial direction and the area was linearly contracted 25% in the initial 5.08 cm of the buffer region. Characteristic outflow boundary conditions were then imposed at the exit. With contraction the flow near the outflow is positive and causes no problems with the characteristic outflow boundary conditions. The effect of varying the contraction and the length of the buffer region was also studied. It was determined that the chosen buffer region and the contraction has negligible effect on the flame dynamics. This is because due to the high swirl the flame is located very close to the fuel exit plane and all the combustion process is completed within 1-2 jet diameter distance from the fuel exit plane.

Results and Discussions

The results of the current LES are discussed in this section. Although both non-reacting and reacting LES were conducted, only the reacting flow results will be discussed in detail.

To obtain statistically stationary results for comparison with the LDV data provided by GEAE the simulations were carried out for over 20 flow-through times and the data were time-averaged using the last 15 flow-through times. Although analysis suggests that the solution has reached stationary state (comparison of results after 10, 15 and 20 flow-through times shows that many but not all flow properties have reached stationary state), we plan to continue these simulations further in time to ensure this. The key limiting condition for such long simulations is the availability of CPU time. The current simulations were carried out on the Cray T3E and typically 90 processors were employed primarily to reduce the turn-around time (for the present problem size, LES could have been conducted using around 24 processors). As shown in Table I the present LES code does scale up quite well on the Cray T3E but the scaleup efficiency degrades if the problem size is too small. Furthermore, the processing speed of around 33 MFLOPS/processor was estimated using this problem size on the 90-processor configuration. Therefore, it is likely that a larger grid will scale up even better and execute at a much faster speed. Since we plan to simulate this combustion flow field using a much higher resolution (e.g, 1-2 million grid points) we will revisit this issue. The 90-processor option was chosen at present as an optimum compromise both from scaleup and availability considerations.

A typical simulation using half million grid points on the CRAY T3E required around 2.2 GB of Memory and around 1,000 single processor hours per flow-through time. Using 90-processors, it was possible to get one flow-through time overnight. As noted above the total cost of such simulations depend on the requirements for stationary state. For example, in the present study, adequate results were obtained for comparison with data after 10 flow-though times although we did carry these simulations out twice as long.

We now discuss some of the characteristic results of these calculations. Figure 2 compares the centerline mean axial velocity decay obtained from non-reacting LES using the two grid resolutions employed so far. Although the general trend and magnitudes are similar, there are some differences. For example, in the near field, the coarser grid result shows numerical fluctuations in the mean velocity. Comparison of the mean and

fluctuating velocity fields at various locations showed similar behavior. The higher resolution grid clustered most of the points in the near field where mixing and combustion is expected to occur. Thus, the results were smoother in the near field. However, in the far field and near the walls even the finer grid show numerical effects. As mentioned before, higher resolution LES is still required to ensure that such grid effects are not contaminating the near field predictions.

Figure 3 compares the non-reacting and reaction centerline mean axial velocity decay using the higher grid resolution. The effect of combustion and heat release can be clearly seen in the reacting flow data as a velocity hump. This is the well known flow acceleration behind a premixed flame that has been seen in many past experimental and numerical studies (e.g., Smith and Menon, 1998). From this figure is can be inferred that the steady state flame is located within 1 jet diameter distance from the fuel exit plane. This location is far upstream of the side injection ports (located at 51mm).

Time averaged vorticity magnitude $|\omega|$ contour plots are shown in Figs.4 (a-d) while two arbitrarily chosen instantaneous vorticity fields are shown in Figs. 5 (a-d) and Figs. 6 (a-d). The plots include one plane perpendicular to z-axis through the combustor centerline and three planes perpendicular to x-axis at three different down stream locations of the fuel exit (x=6 mm, 24 mm, and 78 mm, respectively). The second location at 24 mm is approximately near the steady-state flame location. The swirling incoming premixed jet expands rapidly and results in a forward stagnation point. The unsteadiness of the flow can be clearly seen in the plots (Figs. 5 and 6). Detailed animated visualization of the flow field shows that the high swirl results in a very complex vortex shedding pattern with significant azimuthal structure. The shear layer is quickly broken up into highly stretched (azimuthally) vortex rings. As the vortices impact on the wall secondary vortices of the opposite sign are also generated. This phenomenon is well known. It can also be seen from the instantaneous cross-plane figures that although the vortex rings break down quickly, near the flame (at x=24 mm) there is still significant azimuthal coherence in the vortex structure.

Figure 7 shows the time averaged (a) and instantaneous (b and c) flame kernels. The flame zone has been magnified for comparison but is actually very small relative to the combustor dimensions. The unsteadiness of the shear flow due to swirl also directly affects the flame structure as can be seen in these figures. Comparison of the instantaneous flame and vortical structures show that the flame is located very close to the region of high coherent vorticity. Thus, it is likely that, locally, the flame may be encountering regions of high strain. This coupled with the increased flame curvature seen in the LES results would suggest that stretch effects may be important for such flames. It is well known that high stretch can cause premixed flame extinction and is an area of considerable interest. Although the G-equation model can be used to mimic extinction (for example, by setting the flame speed to zero if the local strain exceeds a pre-specified value) it cannot handle re-ignition (which requires reduction of strain as well as appropriate temperature). These issues can be addressed using relatively simple (single step) chemistry and will be the focus of future investigation.

Figure 8a compares the present LES results with available data on the mean axial velocity decay along the centerline. Both the constant coefficient and the dynamic subgrid model predictions are shown in these figures. Also shown is a LES prediction using the constant coefficient model but with a reduced inflow mean axial velocity (of 103 m/s) similar to the value used by GEAE in their anchored CCD studies. Comparison with data shows reasonable agreement. There is not much difference between the two subgrid approaches before the flame. However, after the flame location (which is around 24 mm) there are some observable differences. It would appear that the dynamic model agrees with the data in the far field better than the constant coefficient model.

As noted above, earlier LES was carried out using a reduced inflow velocity as provided by GEAE (shown in Fig. 8a). This axial inflow velocity (at the center) of 103 m/sec was anchored by GEAE to carry out their optimized CCD calculations. For comparison Fig. 8b shows the results predicted by GEAE using their Anchored CCD approach (Hura et al., 1998; Held et al., 1998a,b). These calculations are done using 60x40x28. As can be seen they obtained good agreement by anchoring the inlet velocity profiles. The LES results shown in Fig. 8a also shows very good agreement without any adjustments to the model. (These results can be further improved by employing the inlet velocity and turbulence profiles which are anchored for LES.) Analysis of the data shows that the present LES predicts the location of the forward stagnation point (59mm from dynamic model LES and 50mm from constant coefficient model LES) in very good agreement with the experimental data (56mm) and the earlier Anchored CCD calculations by GEAE.

Figures 8c and 8d show respectively, the mean axial velocity profiles in the y-direction at x=5.83mm and x=23.94mm. Agreement is again reasonable at x=5.83 mm. At the second location LES predictions are not in

good agreement. even though the magnitude is reasonable. The experiments suggest a peak at y=0 but the LES data shows a peak further away from the center. The earlier calculations using Anchored CCD modeling by GEAE also showed results somewhat similar to the present calculations.

Figures 9a and 9b show the mean radial velocity profiles in the y-direction at x=5.83mm and x=23.94mm, respectively. Comparison with LDV data shows reasonable agreement. Both the magnitude and the trend of the velocity profile is accurately predicted by the LES. The lack of resolution in the far field (near the walls) shows up as numerical noise in the far field data. It can be seen that the dynamic model has more noise than the constant coefficient model. As noted above, the very coarse resolution in the far field causes large variation in the dynamic model coefficient. However, it appears that in the near field where the grid is reasonably fine, both subgrid approaches behave very similar.

Figures 10a and 10b shows the mean tangential velocity profiles in the z-direction at x=5.83mm and x=23.94mm, respectively. Again, the agreement with experimental data is considered reasonable considering the resolution employed. There are no appreciable differences between the two subgrid approaches.

These comparisons suggest that at least for such coarse grid LES, the constant coefficient model is probably acceptable. Note that, dynamic model is much more expensive and therefore, using the constant coefficient model will also reduce the overall computational cost. It is not yet clear if the dynamic model will give improved predictions when higher grid resolution is employed. This issue still remains to be addressed.

Many other flow properties were computed and stored during the LES. Such flows properties include all second- and third-order correlations. However, these properties have not yet been fully analyzed. Here, we compare some of the predicted results for turbulence intensity. There are no experimental data available for these properties so comparison is not possible. However, given the reasonable agreement of the mean flow data, the predicted turbulence intensity variations are also likely to be similar to the experimental case.

Figures 11a, 11b and 11c show respectively, the axial, radial and tangential velocity fluctuation intensity profiles at the same axial location of x=23.94. Both the reacting and non-reacting data are shown in these figures. The axial velocity fluctuation intensity for the reacting case shows significant magnitude in the shear layer region where the flame is located. The radial and tangential fluctuation intensities are also quite large and comparable to the axial intensities. Interestingly, the tangential intensity (Fig. 11c) shows very high values near the outer region for the reacting case. However, the accuracy of the present LES results in the outer regions remains to be determined since the current resolution there is considered too coarse.

Conclusions

This paper has reported on the application of LES to study premixed combustion in a device that is part of a real combustor. Thus, the geometry and flow conditions are chosen to match actual operational condition for the General Electric's lean premixed dry low NOx LM-6000 combustor. The goal of this exercise was to evaluate the feasibility of carrying out "engineering" LES of actual hardware. To achieve this goal, some simplifications such as very coarse grid resolution was needed to reduce the computational time. The computational time was also considerably reduced by using the thin flame model for premixed combustion. However, analysis of the flow conditions suggest that the thin flame model is actually a good approximation for the real case provided issues such as extinction and re-ignition are not considered. The LES were carried out using both constant coefficient and dynamic models for the subgrid kinetics energy. Comparison of the computed results with experimental data indicate very good agreement in spite of relatively coarse grid resolution employed in the LES. These results provide significant confidence that advanced parallel LES capability for design studies of practical interest is feasible in the near future.

Acknowledgments

This work was supported in part by the Air Force Office of Scientific Research Focused Research Initiative contract F49620-95-C-0080, monitored by General Electric Aircraft Engine Company, Cincinnati, Ohio and by the Army Research Office Multidisciplinary University Research Initiative grant DAAH04-96-1-0008. Computations were carried out under the DoD HPC Grand Challenge Project at NAVO, Stennis Space Center and ARC, Huntsville.

References

Cheng, R. K. (1995) "Velocity and scalar characteristics of premixed turbulent flames stabilized by weak swirl," *Combustion and Flame* **101**, pp. 1-14.

Fureby, C., Tabor, G., Weller, H. G., and Gosman, A. D. (1997) "A comparative study of subgrid scale models in homogeneous isotropic turbulence," *Physics of Fluids* **9**, pp. 1416-1429.

Held, T. J., Mongia, H. C., and Tonouchi, J. H. (1998) "Application of a micro-/macro-mixing two reactor model to a single cup low-emissions combustor," ASME Paper No. 98-GT-218.

Held, T. J., and Mongia, H. C. (1998) "Application of a partially premixed laminar flamelet model to a low-emission gas turbine combustor," ASME Paper No. 98-GT-217.

Hura, H. S., Joshi, N. D., Mongia, H. C., and Tonouchi, J. (1998) "Dry low emission premixer CCD modeling and validation," ASME Paper No. 98-GT-444.

Kerstein, A. R., Ashurst Wm., T. and Williams F. A. (1988) "The Field Equation for Interface Propagation in an Unsteady Homogeneous Flow Field," *Physical Review* A **37**, pp. 2728-2731.

Kim, W.-W. and Menon, S. (1995) "A new dynamic one-equation subgrid-scale model for large-eddy simulations," AIAA 95-0356.

Kim, W.-W. and Menon, S. (1997) "Application of a localized dynamic subgrid-scale model to turbulent wall-bounded flows," AIAA 97-0210.

Kim, W.-W. and Menon, S. (1999) "LES of premixed turbulent reacting flows in a highly-swirling combustor," submitted to present at 37th AIAA Aerospace Sciences Meeting, Reno, NV, January 11-14, 1999.

Menon, S. and Calhoon, W. (1996) "Subgrid mixing and molecular transport modeling for large-eddy simulations of turbulent reacting flows," Symposium (International) on Combustion, **26**, pp. 59-66.

Menon, S. and Jou, W.-H. (1991) "Large-eddy simulations of combustion instability in an axisymmetric ramjet combustor," *Combustion Science and Technology* **75**, pp. 53-72

Menon, S. and Kim, W.-W. (1996) "High Reynolds number flow simulations using the localized dynamic subgrid-scale model," AIAA 96-0425.

Nelson, C. C. and Menon, S. (1998) "Unsteady simulations of compressible spatial mixing layers," AIAA 98-0786

Peters, N. (1998) "The turbulent burning velocity for large scale and small scale turbulence," *Submitted to Journal of Fluid Mechanics.*

Pocheau, A. (1994) "Scale Invariance in Turbulent Front Propagation," *Physical Review* E. **49**, pp. 1109-1122.

Smith, T. M. and Menon, S. (1998) "Subgrid Combustion Modeling for Premixed Turbulent Reacting Flows," AIAA 98-0242.

Yakhot, V. (1988) "Propagation velocity of premixed turbulent flames," *Combustion Science and Technology* **60**, pp. 191-214.

Overall Grid	# PEs	$T_{communication}$	$T_{compute}$	T_{total}
CRAY T3E (Secs)				
96x64x80	8	1.20985875	9.984778125	11.19463688
	16	0.687654344	5.030144063	5.717798406
	32	0.478368688	2.593220781	3.071589469
	64	0.337139852	1.355396953	1.692536805
	128	0.225933906	0.749989961	0.975923867
SGI ORIGIN 2000 (Normalized by T3E data)				
96x64x80	8	0.571	0.488	0.497
	16	0.553	0.460	0.471
	32	0.841	0.528	0.577

Table 1: Timings for the 3D LES code with one species (G eqn.) on different parallel systems. Note that I/O timing is not included.

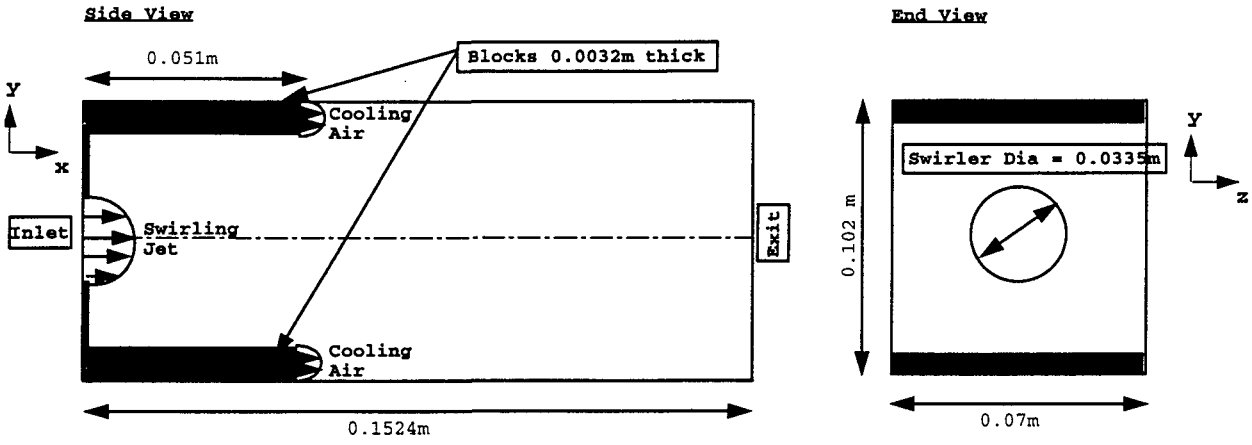

Figure 1: Schematic of the GE low NOx Premixed Combustor.

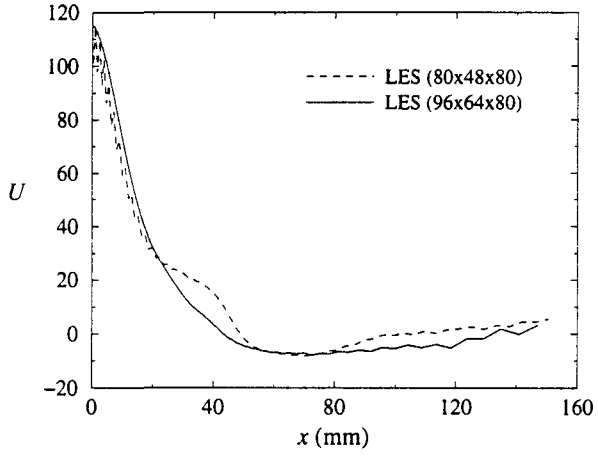

Figure 2: Comparison of the axial velocity variations along the combustor centerline obtained from LES using different resolutions.

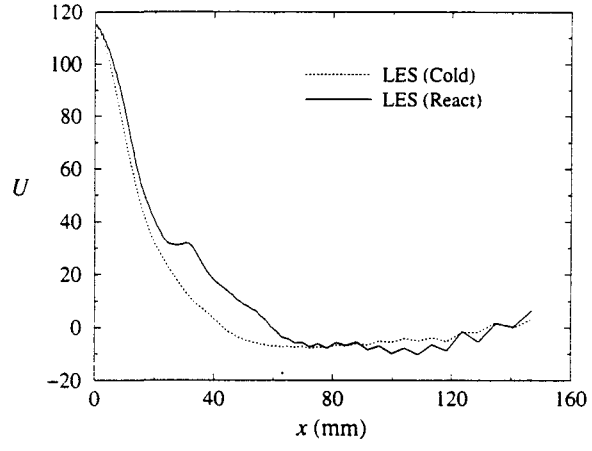

Figure 3: Comparison of the axial velocity variations along the combustor centerline obtained from LES of non-reacting and reacting flows.

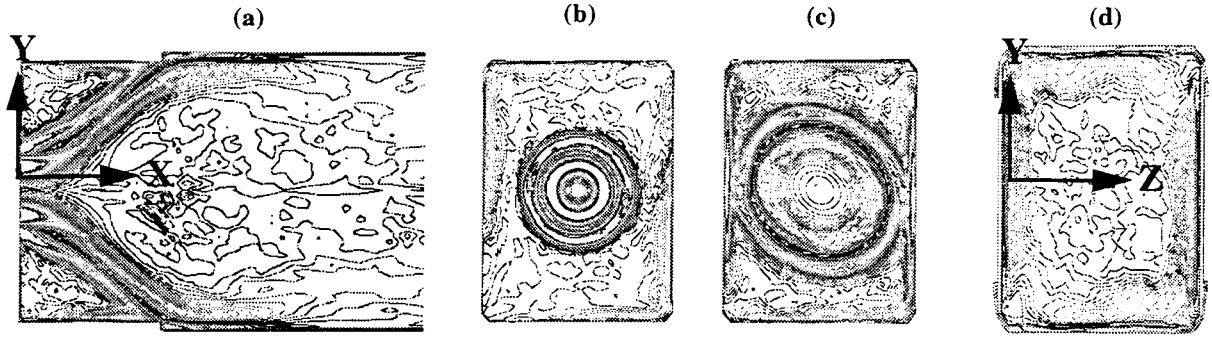

Figure 4: Averaged vorticity magnitude contours. (a) Side view, (b) End view (x=6 mm), (c) End view (x=24 mm) and (d) End view (x=78 mm).

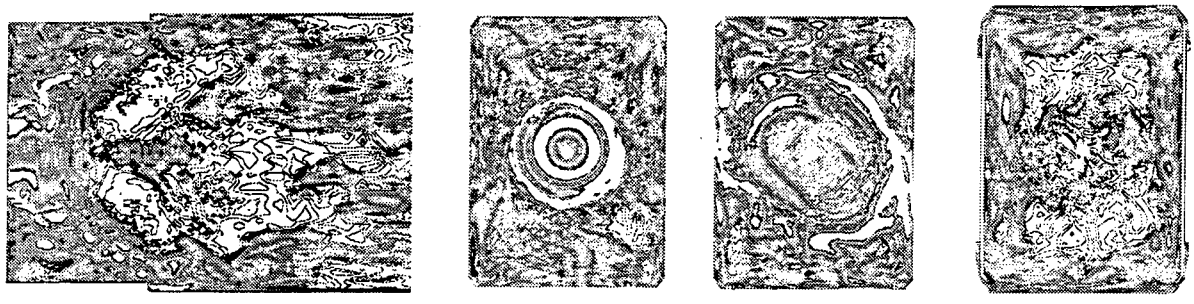

Figure 5: Instantaneous vorticity magnitude contours. (a) Side view, (b) End view (x=6 mm), (c) End view (x=24 mm) and (d) End view (x=78 mm).

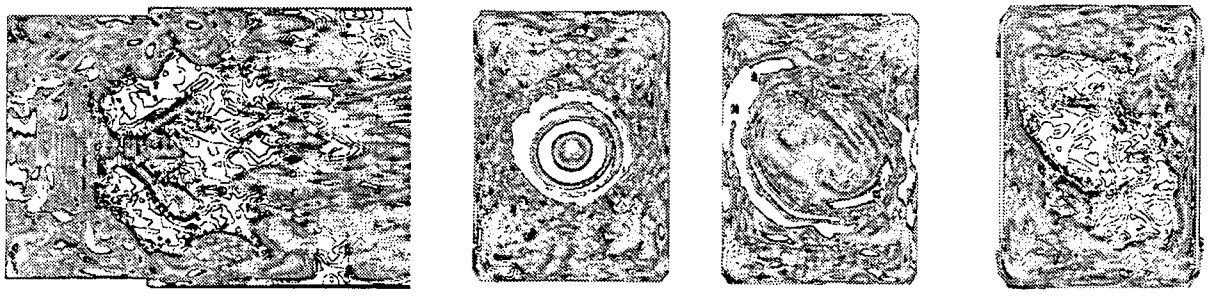

Figure 6: Instantaneous vorticity magnitude contours. (a) Side view, (b) End view (x=6 mm), (c) End view (x=24 mm) and (d) End view (x=78 mm).

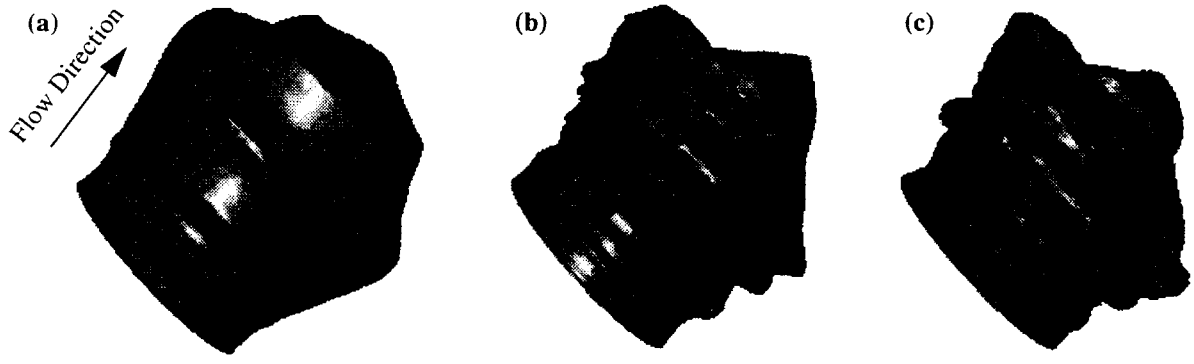

Figure 7: Flame kernel (a) Time Averaged; (b) and (c) Two instantaneous snap shots.

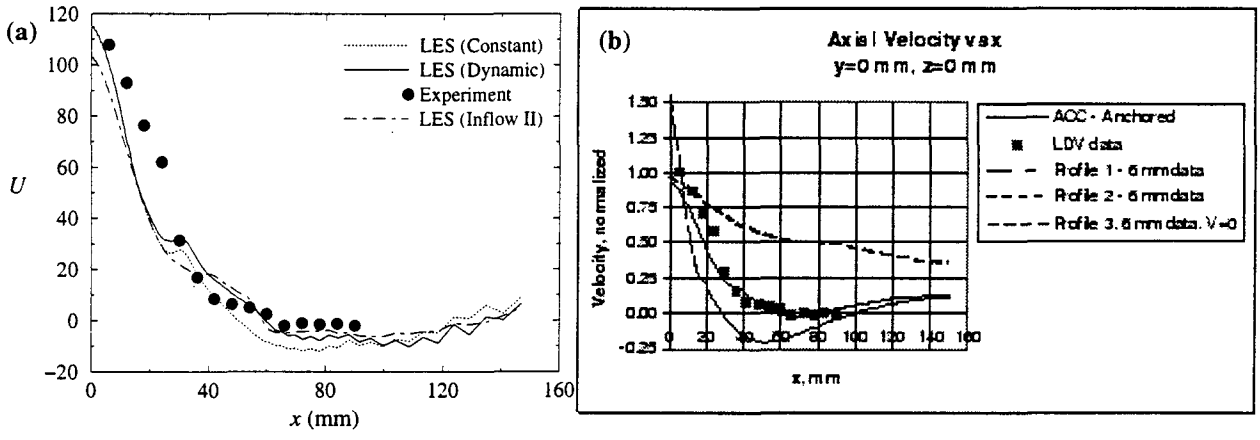

Figure 8: Comparison of the predicted axial velocity along the combustor centerline and the experimental data. (a) LES and (b) Anchored CCD by GEAE.

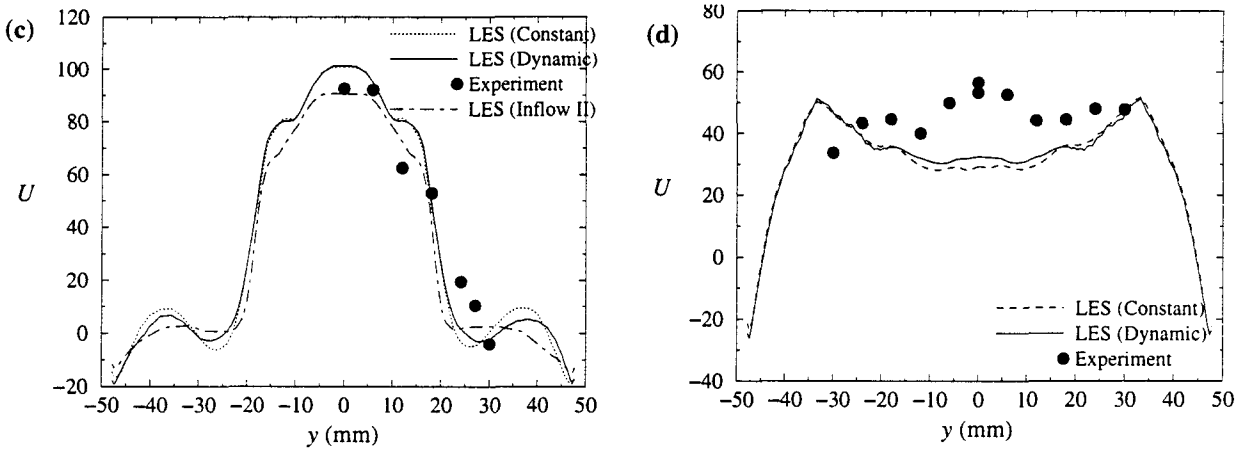

Figure 8: Comparison of the predicted axial velocity and the experimental data along the y-axis (c) 5.83mm and (d) 23.94mm downstream of the inlet.

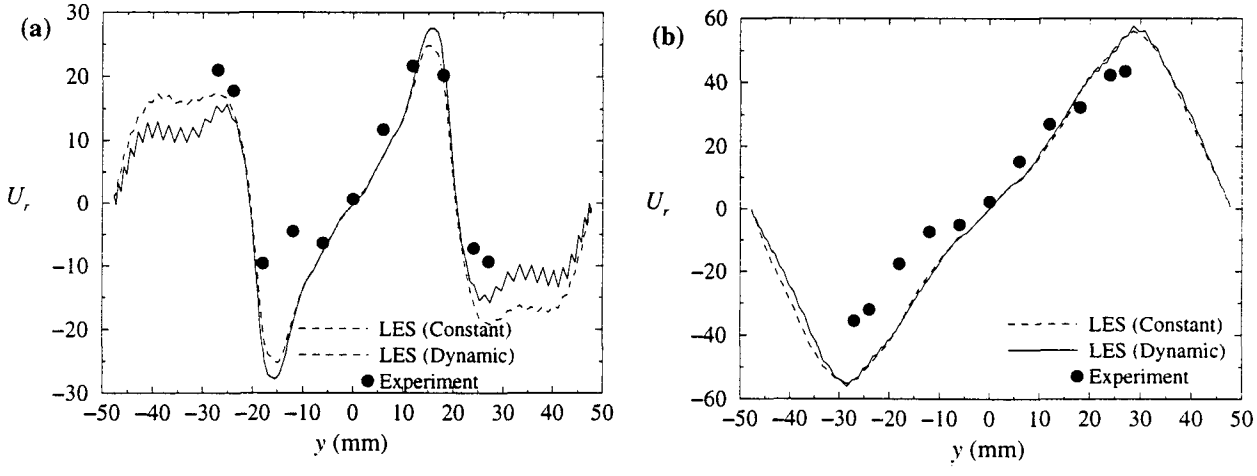

Figure 9: Comparison of the predicted radial velocity and the experimental data along the y-axis (a) 5.83mm and (b) 23.94mm downstream of the inlet.

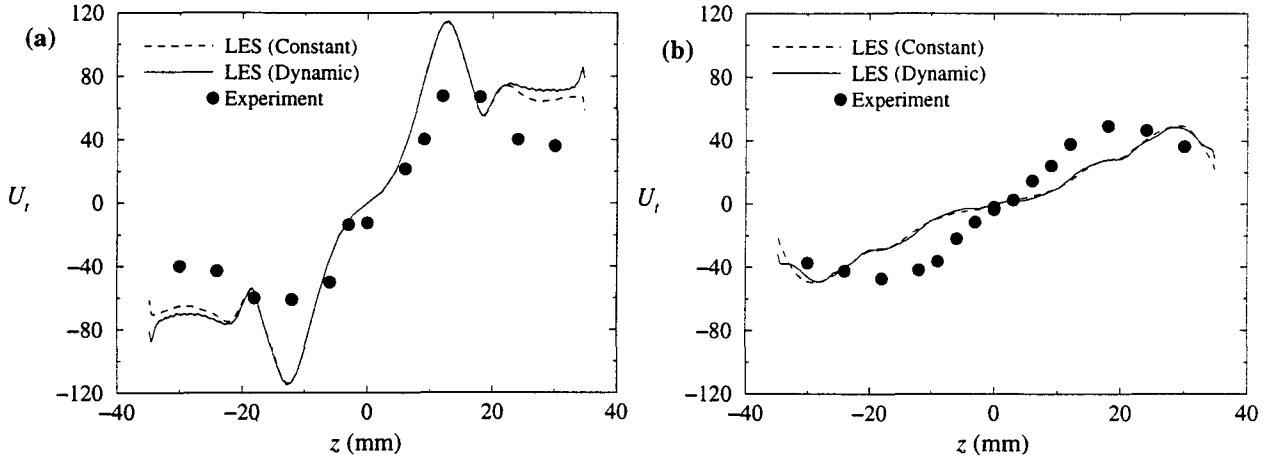

Figure 10: Comparison of the predicted tangential velocity and the experimental data along the z-axis (a) 5.83mm and (b) 23.94mm downstream of the inlet.

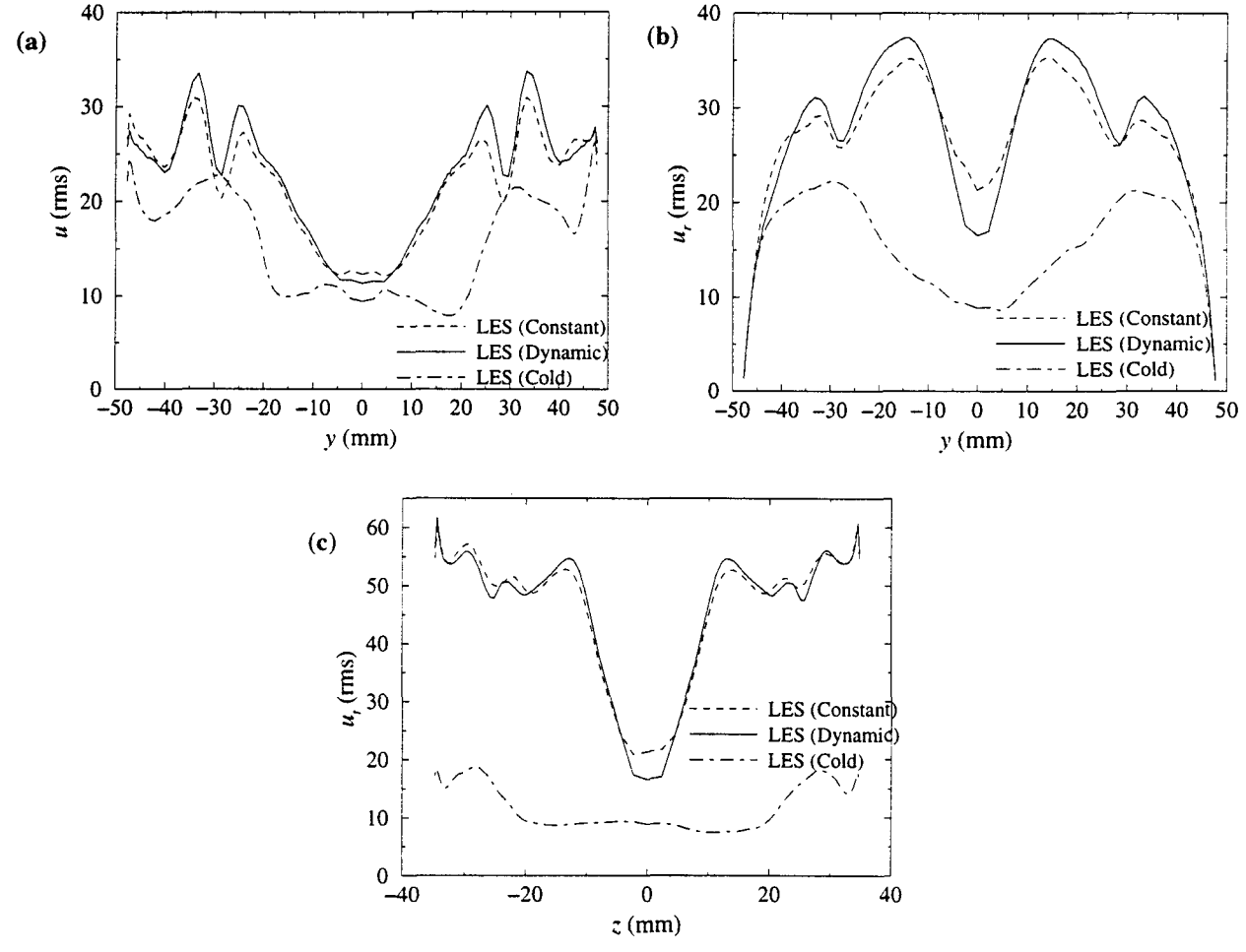

Figure 11: Turbulence intensities at 23.94mm downstream of the inlet. (a) axial, (b) radial, and (c) tangential components.